Communications in Theoretical Physics

Commun. Theor. Phys. **77** (2025) 055504 (13pp) https://doi.org/10.1088/1572-9494/ad98fe
CSTR: 32041.14.CTP.ad98fe

Dromion structure in (2+1)-dimensional modulated positron-acoustic waves in a non-Maxwellian magnetoplasma

Aljawhara H Almuqrin[1], Alim[2], B B Mouhammadoul[2], C G L Tiofack[3], A Mohamadou[4,5], Sherif M E Ismaeel[6], Weaam Alhejaili[7] and S A El-Tantawy[8,*]

[1] Department of Physics, College of Science, Princess Nourah bint Abdulrahman University, PO Box 84428, Riyadh 11671, Saudi Arabia
[2] Higher Teachers' Training College, University of Maroua, PO Box 55, Maroua, Cameroon
[3] Faculty of Sciences, University of Maroua, PO Box 814, Maroua, Cameroon
[4] National Advanced School of Engineering, University of Maroua, PO Box 46, Maroua, Cameroon
[5] The Max Planck Institute for the Physics of Complex Systems, Nothnitzer Strasse 38, 01187, Dresden, Germany
[6] Department of Physics, College of Science and Humanities in Al-Kharj, Prince Sattam bin Abdulaziz University, Al-Kharj 11942, Saudi Arabia
[7] Department of Mathematical Sciences, College of Science, Princess Nourah bint Abdulrahman University, PO Box 84428, Riyadh 11671, Saudi Arabia
[8] Department of Physics, Faculty of Science, Al-Baha University, Al-Baha, PO Box 1988, Saudi Arabia

E-mail: samireltantawy@yahoo.com

Received 19 August 2024, revised 17 November 2024
Accepted for publication 18 November 2024
Published 12 February 2025

Abstract

This study investigates the dromion structure within the context of (2+1)-dimensional modulated positron-acoustic waves in a magnetoplasma consisting of inertial cold positrons and inertialess nonthermal hot electrons and positrons as well as stationary positive ions. The reductive perturbation approach reduces the fluid governing equations to the plasma model to a Davey–Stewartson system. This study provides a detailed analysis of the influence of many related plasma parameters, including the density ratio of hot and cold positrons, the external magnetic field strength, the nonthermal parameter and the density ratio of electrons and cold positrons, on the growing rate of instability. Using the Hirota Bilinear method, it is found that the system supports some exact solutions, such as one- and two-dromion solutions. The change of plasma parameters significantly enhances the characteristics of dromion solutions. The elastic and inelastic collisions between two dromions are discussed at different times. The relevance of this study can help us to understand the various types of collision between energetic particles in confined plasma during the production of energy by thermonuclear fusion.

Keywords: Davey–Stewartson equations, positron-acoustic waves, modulational instability, magnetoplasmas, dromion soliton

1. Introduction

In recent times, there has been a significant surge in researchers' interest in investigating positron-acoustic waves (PAWs) in unmagnetized plasma environments and plasmas subjected to magnetic fields (MFs). The PAWs are distinguished by the presence of two separate temperature positron components. The provision of inertia is attributed to the mass of cold positrons, whereas the thermal pressure exerted by hot positrons (electrons) is the restoring force. However, it is assumed that the heavy ions are stationary and only sustain the quasi-neutrality condition at equilibrium.

* Author to whom any correspondence should be addressed.

Several studies have explored the nonlinear characteristics of PAWs [1–5]. For instance, Rahman *et al* [6, 7] and Uddin *et al* [8, 9] examined the characteristics of nonlinear propagation of nonplanar Gardner solitons, specifically in cylindrical and spherical geometries, associated with PAWs in a four-component plasma system. These investigations have revealed that the properties of nonplanar PAWs, such as amplitude, polarity and speed, differ from those of planar geometry. In addition, the nonlinear positron-acoustic (PA) shock waves within a high-density plasma system consisting of non-relativistic and ultra-relativistic degenerate electrons, cold (hot) positrons and stationary positively charged ions have been examined [10]. Tribeche *et al* [11] conducted a theoretical investigation in order to demonstrate the presence and potential manifestation of PA solitary waves (PASWs) involving the dynamics of mobile cold positrons. Furthermore, the study examined the presence of PA double layers (DLs) within a four-component plasma model. The findings revealed that the plasma model accommodates compressive and rarefactive PA-DLs. Moreover, the characteristics of nonlinear PA shock waves have been investigated in an unmagnetized plasma composed of cold positrons, immobile positive ions, and electrons with a Boltzmann distribution [12]. The analysis considers both unbounded planar geometry and bounded nonplanar geometry. For this purpose, the authors [12] applied the reductive perturbation method (RPM) to derive the nonplanar Korteweg–de Vries–Burgers equation to investigate the characteristics of PASWs. In a recent study conducted by Saha *et al* [13], the authors examined the propagation of PAWs in an unmagnetized plasma. The findings of this investigation offer valuable insight into comprehending the intricacies of nonlinear propagation within the auroral area. Furthermore, Saha and his research group [14, 15] have documented the influence of superthermal on PAWs in several plasma models.

In addition to the global Coulomb interaction of all the charged species, the particles, taken two by two, can interact [16, 17]. These direct interactions between particles give rise to transfers of momentum, energy, or even more complex reactions such as ionization, excitation and recombination [18, 19]. They are grouped under the general term of collisions and are characterized at the microscopic scale by collision cross-sections. Two distinct types of collisions exist, overtaking collision (OC) and head-on collision (HOC), which can be differentiated based on their propagation direction. Concerning the OC, the waves propagate in a parallel path but with varying velocities, whereas in the HOC, the colliding waves propagate in opposite directions. The HOC of both solitary and shock waves has been investigated in several plasma models through the application of the Poincaré–Lighthill–Kuo approach [20–25]. On the other hand, Hirota's method [26–29] or the inverse scattering transformation method [30] are considered for investigating the OC. Saha *et al* [31] used Hirota's bilinear method to investigate the multi-soliton solution in a complex plasma model. Furthermore, they derived the phase shift that arises after the collision of these solitons. Moreover, the latter method was applied to study the OC of two solitons in a non-Maxwellian unmagnetized plasma with nonextensive electrons and Maxwellian positrons. The obtained findings highlight the significant influence of the nonextensive parameter on both the generation of the two solitons and the characteristics of their phase shifts after collision. Moreover, Singh *et al* [32] examined the OC among multisolitons in a non-Maxwellian electron-positron-ion magnetoplasma with nonthermal electrons and positrons. The OC of nonplanar electron-acoustic solitons has also been investigated in an unmagnetized plasma consisting of inertial cold electrons and inertialess hot superthermal electrons, as well as stationary ions [33]. Despite the fact that soliton collisions are considered to be one of the wonderful and fascinating phenomena of nonlinear wave dynamics, the OC of PAWs is less investigated. We can cite the work of [34], where the author examined the inelastic collision of PAWs in four-component plasmas and found that the plasma physical parameters play a major role in changing the amplitude of PAWs.

Over the decades, most of the studies related to nonlinear PAWs were focused on the Maxwellian electrons and positrons [35, 36]. However, observations of astrophysical plasmas give some information about the nonthermal plasma, which is distinguished by the presence of an elongated tail in the high-energy domain [37–39]. With the help of a weak MF, the solar wind leads to the creation of nonthermal ions in the atmosphere of planets [40–42]. There remains a multitude of other sources that show the existence of fluxes of nonthermal electrons (ions). Moreover, the genesis and mechanism of nonthermal particle production in space plasma have always impressed researchers [43–46]. Hence, it is crucial to examine the influence of nonthermal positrons on the properties of nonlinear phenomena in a plasma with nonthermal positrons.

Recently, the general class of multidimensional soliton solutions, called dromions, has drawn considerable attention in plasma physics [47]. A well-known multidimensional system that admits dromion solutions is the Davey–Stewartson (DS) equation. Many researchers have investigated dromion structures in various plasma models. For example, 2D modulated ion-acoustic waves (IAWs) have been studied in electronegative plasma by Panguetna *et al* [48]. By applying the RPM, they showed that the basic fluid equations could be transformed into a (2+1)-dimensional DS system, and they obtained several solutions for these equations, namely one- and two-dromion solutions. Modulated IAWs were analyzed through the activation of modulation instability (MI) within the framework of (3+1)-dimensional DS equations in [49] where the negative ion concentration ratio's impact was observed through the growth rate of instability. Note that MI is a nonlinear phenomenon that arises when a small modulating perturbation acting on a plane wave propagating through a nonlinear medium results in exponential wave amplitude growth. Bedi *et al* [50] derived the DS equations in hot electron plasma, which obeys Kappa distribution. They found the best analogy that exists between the DS equations and the nonlinear Schrödinger equation. Jianping *et al* [51] used the dynamical system method to

obtain periodic, solitary wave solutions, as well as unbounded wave solutions governed by the DS equations.

Nevertheless, the investigation of MI and the OC of dromion-like solitons of PAWs in magnetized plasma with Cairns nonthermal statistic on the framework of DS equations has not been reported so far, even if PAWs are omnipresent in the Universe. Moreover, studying the effects of the nonthermal parameter helps researchers understand non-Maxwellian plasmas, which are common in various natural and laboratory settings. This insight is crucial for advancing our knowledge of plasma physics and for applications such as controlled fusion and astrophysical research. Thus, based on the DS equations, our present paper aims to examine the criteria for the appearance of dromion-like solitons of PAWs by MI and the OC of the dromion structures in this plasma. In addition, the relevant plasma parameters' response to the stability condition and the characteristics of localized structures are reported. Our study will provide new information on the dynamics of dromions for PAW plasmas. Our results will thus contribute to a better understanding of localized multidimensional phenomena as well as their interactions in this specific type of plasma.

The study is extended as follows. In section 2, we present the model equations. We derive the DS equations in section 3. In section 4, the analysis of MI is addressed. The localized structures, such as dromion-like solitons, are discussed in section 5. A brief discussion is provided in the last section.

2. Theoretical fluid model and equations of motion

Here, we consider a magnetoplasma model having inertialess nonthermal hot electrons and positrons and inertial cold positrons as well as stationary positive ions. The influence of the MF has also been considered. The quasi-neutrality condition can be expressed in the following manner: $n_{cp0} + n_{hp0} + n_{i0} = n_{he0}$, with n_{cp0}, n_{hp0}, n_{i0}, and n_{he0}, which indicates the unperturbed number densities of cold(hot) positrons, stationary ions and hot electrons, respectively. The MF $\hat{B}_0$ is assumed to lie in the z-direction, i.e, $\hat{B}_0 = B_0\hat{z}$ with $\hat{z}$ is a unit vector in the direction of the z-axis. The fluid model of the plasma, consisting of quantities, such as density and average velocity around each position, is described by [2, 3]:

◇ the continuity equation, which expresses the conservation of the number of particles,

$$\frac{\partial}{\partial t}n_{cp} + \nabla\ (n_{cp}U_{cp}) = 0, \tag{1}$$

◇ the momentum equation which describes the fluid equation of motion,

$$\frac{\partial}{\partial t}U_{cp} + (U_{cp}\,\nabla)U_{cp} = -\nabla\ \Phi - U_{cp} \times\ B_0\,\hat{z}, \tag{2}$$

◇ the Poisson's equation, which highlights the conservation of the electric charges in plasma,

$$\nabla^2\Phi = \mu_e\, n_{he} - \mu_p\, n_{hp} + \varpi,$$
$$\varpi = -n_{cp} - \mu_e + \mu_p + 1. \tag{3}$$

Here, n_{cp} represents the number density of cold positron scaled by n_{cp0}. $U_{cp} = u\hat{x} + v\hat{y}$, where u and v denote the velocities of the cold positron fluid scaled by the PA velocity $C_{cp} = \left(\frac{k_B T_{he}}{m_p}\right)^{1/2}$, ($k_B$ indicates the Boltzmann constant, $T_{he}(T_{hp})$ represents the hot electron (positron) temperature, m_p being the positron's mass). The electrostatic potential Φ is scaled by the quantity $\frac{k_B T_{he}}{e}$, with e the magnitude of the electron charge. The other parameters are given by $\mu_e = n_{he0}/n_{cp0}$ and $\mu_p = n_{hp0}/n_{cp0}$. The time is scaled by the plasma period $\omega_{cp}^{-1} = (m_p/4\pi e^2 n_{cp0})^{1/2}$, whereas the space variables are in the unit of the Debye length $\lambda_D = \left(\frac{k_B T_{he}}{4\pi e^2 n_{cp0}}\right)^{1/2}$ and $\omega_{c1} = \frac{\Omega_1}{m_p}$ denotes the MF scaled by the gyro-frequency $\Omega_1 = \frac{|e|B_0}{m_p}$. According to Cairn's nonthermal statistic [52–54], the number densities of hot positrons (via n_{hp}) and hot electrons (via n_{he}) are given as:

$$n_{hp} = (\rho\,\sigma^2\Phi^2 + \Phi\,\rho\,\sigma + 1)e^{-\sigma\,\Phi}, \tag{4}$$

$$n_{he} = (\rho\,\Phi^2 - \Phi\,\rho + 1)e^{\Phi}, \tag{5}$$

where the temperature's ratio of hot electrons to hot positrons reads $\sigma = \frac{T_{he}}{T_{hp}}$. The quantity $\rho = \frac{4\alpha}{(1+3\alpha)}$ estimates the deviation from the thermalization state. However, the nonthermal parameter ρ is in the range $0 < \rho < 1.3$ and ($\alpha > 0$) in the practical situation [55]. The proportion of the fastest energetic electrons is determined by the parameter α. When $\rho \to 0$, the positron (electron) density reduces to the well-known Boltzmann distribution. From equations (1)—(3), with the above assumptions one can obtain the dimensionless continuity, momentum and Poisson's equations:

$$\frac{\partial}{\partial t}n + \frac{\partial}{\partial x}(nu) + \frac{\partial}{\partial y}(nv) = 0, \tag{6}$$

$$\frac{\partial}{\partial t}u + u\frac{\partial}{\partial x}u + v\frac{\partial}{\partial y}u + \frac{\partial}{\partial x}\Phi - \omega_{c_1}v = 0, \tag{7}$$

$$\frac{\partial}{\partial t}v + u\frac{\partial}{\partial x}v + v\frac{\partial}{\partial y}v + \frac{\partial}{\partial y}\Phi + \omega_{c_1}u = 0, \tag{8}$$

$$\frac{\partial^2}{\partial x^2}\Phi + \frac{\partial^2}{\partial y^2}\Phi + = \gamma_2\Phi^2 + \gamma_1\Phi - n + 1, \tag{9}$$

with

$$\gamma_1 = (1 - \rho)(\mu_e\sigma + \mu_e),$$
$$\gamma_2 = \frac{(\mu_e - \mu_p\sigma^2)}{2},$$
$$\gamma_3 = \frac{(1+3\,\rho)(\sigma^3\mu_p + \mu_e)}{6}. \tag{10}$$

Before going to the numerical part of this work, we note that the range of parameters used here are [3, 54, 56, 57]: $\mu_e = 1.5 - 3.5$; $\mu_p = 0.1 - 0.3$; $0 < \rho < 1.3$ and $\sigma = 2 - 2.6$, which satisfies numerous plasma models from the laboratory to the plasma environment such as auroral acceleration regions, solar wind and cosmic rays.

3. Formation of the Davey–Stewartson equations

The standard RPM is the most used method of its type in the literature to obtain many nonlinear differential equations that govern particle dynamics in the fluid medium. Thus, it is applied here to derive the DS equations in our fluid model. The following stretching of independent variables is employed with respect to this method [58]:

$$\xi = \epsilon(x - v_g t), \quad \eta = \epsilon\, y, \quad \tau = \epsilon^2 t, \tag{11}$$

where ϵ, ($\epsilon \ll 1$) is a small parameter that measures the strength of nonlinearity and v_g is the group velocity of the PAWs. This is determined in the next section according to the solvability condition. Moreover, the scalar quantities $n(x, y, t)$, $u(x, y, t)$, $v(x, y, t)$ and $\Phi(x, y, t)$ in the above relations can be written as:

$$n = 1 + \sum_{s=1}^{\infty} \epsilon^s \sum_{q=-\infty}^{\infty} n_q^{(s)}(\xi, \eta, \tau) S_1(x, t)^q, \tag{12}$$

$$U = \sum_{s=1}^{\infty} \epsilon^s \sum_{q=-\infty}^{\infty} \begin{pmatrix} u_q^{(s)}(\xi, \eta, \tau) \\ v_q^{(s)}(\xi, \eta, \tau) \end{pmatrix} S_1(x, t)^s, \tag{13}$$

$$\Phi = \sum_{s=1}^{\infty} \epsilon^s \sum_{q=-\infty}^{\infty} \Phi_q^{(s)}(\xi, \eta, \tau) S_1(x, t)^q, \tag{14}$$

where $S_1(x, t)^q = \mathrm{e}^{\mathrm{i}\, q(k\, x - \omega\, t)}$ with k and ω being the scaled wavenumber and frequency of the carrier wave, respectively. Thus, the relationship between the quantities $(n_q^{(s)})^* = n_{-q}^{(s)}$, $(u_q^{(s)})^* = u_{-q}^{(s)}$, $(v_q^{(s)})^* = v_{-q}^{(s)}$ and $(\Phi_q^{(s)})^* = \Phi_{-q}^{(s)}$ must be satisfied. By substituting equations (12)–(14) into equations (6)–(9), one can easily obtain the following algebraic equations:

$$\begin{aligned} -\mathrm{i} n_1^{(1)}\, \omega - u_1^{(1)}\, k &= 0, \\ \mathrm{i}\Phi_1^{(1)}\, k - \mathrm{i} u_1^{(1)}\, \omega - \omega_{c_1}\, v_1^{(1)} &= 0, \\ -\mathrm{i} v_1^{(1)}\, \omega + \omega_{c_1} u_1^{(1)} &= 0, \\ -k^2 \Phi_1^{(1)} - \Phi_1^{(1)}\, \gamma_1 + n_1^{(1)} &= 0. \end{aligned} \tag{15}$$

Thus, their corresponding solutions are giving as:

$$\begin{aligned} \Phi_1^{(1)} &= \frac{n_1^{(1)}}{k^2 + \gamma_1}, \qquad u_1^{(1)} = -\frac{n_1^{(1)} k\omega}{(k^2 + \gamma_1)(-\omega^2 + \omega_{c_1}^2)}, \\ v_1^{(1)} &= \frac{-\mathrm{i} n_1^{(1)} \omega_{c_1}^2 k}{(k^2 + \gamma_1)(\omega^2 - \omega_{c_1}^2)}. \end{aligned} \tag{16}$$

Then, the dispersion relation for the PAWs reads:

$$\omega^2 = \frac{k^2}{k^2 + \gamma_1} + \omega_{c_1}^2.$$

When the MF is neglected ($\omega_{c_1} = 0$), the dispersion relation reaches to the same relation already found in [57]. Now, the second-order mode and first harmonic ($s = 2$ and $q = 1$), gives the following relations:

$$\begin{aligned} &(k^2 + \gamma_1)^2 n_1^{(2)} - (k^2 + \gamma_1)^3\, \Phi_1^{(2)} + 2\,\mathrm{i}(k^2 + \gamma_1) k \frac{\partial}{\partial \xi} n_1^{(1)} = 0, \\ &\mathrm{i}\,(k^2 + \gamma_1)\, k\, \omega_{c_1}\, v_g (\omega^2 - \omega_{c_1}^2) \frac{\partial}{\partial \xi}\, n_1^{(1)} + (\omega^4 + \omega_{c_1}^4) \\ &\times (k^2 + \gamma_1) \frac{\partial}{\partial \eta} n_1^{(1)} \\ &-\mathrm{i}\omega\, (k^2 + \gamma_1)^2 (\omega - \omega_{c_1})^2 (\omega + \omega_{c_1})^2 v_1^{(2)} \\ &+\omega_{c_1} (\omega - \omega_{c_1})^2 (\omega + \omega_{c_1})^2 (k^2 + \gamma_1)^2 u_1^{(2)} = 0, \\ &\mathrm{i}\, k\, (k^2 + \gamma_1)^2 (\omega + \omega_{c_1})^2 (\omega - \omega_{c_1})^2\, \Phi_1^{(2)} \\ &-(k\omega\, v_g - \omega^2 + \omega_{c_1}^2)(k^2 + \gamma_1)(\omega^2 - \omega_{c_1}^2) \frac{\partial}{\partial \xi}\, n_1^{(1)} \\ &-\omega_{c_1} (\omega - \omega_{c_1})^2 (\omega + \omega_{c_1})^2\, (k^2 + \gamma_1)^2 v_1^{(2)} \\ &-\mathrm{i}\omega\, (k^2 + \gamma_1)^2 (\omega - \omega_{c_1})^2 (\omega + \omega_{c_1})^2 u_1^{(2)} = 0, \\ &-\mathrm{i}(k^2 + \gamma_1)\, k\, (\omega^2 - \omega_{c_1}^2) u_1^{(2)} + \mathrm{i}(k^2 + \gamma_1)\omega\, (\omega^2 - \omega_{c_1}^2) n_1^{(2)} \\ &+((k^2 + \gamma_1)\, v_g (\omega^2 - \omega_{c_1}^2) - k\omega) \frac{\partial}{\partial \xi} n_1^{(1)} + \mathrm{i}\omega_{c_1}\, k \frac{\partial}{\partial \eta} n_1^{(1)} = 0. \end{aligned} \tag{17}$$

The solutions of the system (17) are obtained below:

$$\begin{aligned} \Phi_1^{(2)} &= \frac{2\,\mathrm{i}k \frac{\partial}{\partial \xi} n_1^{(1)}}{(k^2 + \gamma_1)^2} + \frac{n_1^{(2)}}{k^2 + \gamma_1}, \\ u_1^{(2)} &= -\frac{\omega_{c_1} \frac{\partial}{\partial \eta} n_1^{(1)} + n_1^{(2)} k\omega}{-k^2\omega^2 + \omega_{c_1}^2 k^2 - \omega^2\gamma_1 + \gamma_1\omega_{c_1}^2} + \frac{\mathrm{i}\left(\frac{\partial}{\partial \xi} n_1^{(1)}\right)(F_1 + F_2)}{F3 + F4}, \\ v_1^{(2)} &= \frac{\mathrm{i}\left(\frac{\partial}{\partial \eta} n_1^{(1)}\right)\omega + \mathrm{i}k\omega_{c_1} n_1^{(2)}}{-k^2\omega^2 + \omega_{c_1}^2 k^2 - \omega^2\gamma_1 + \omega_{c_1}^2\gamma_1} + \frac{\omega_{c_1} F_5 \frac{\partial}{\partial \xi} n_1^{(1)}}{F_3 + F_4}. \end{aligned} \tag{18}$$

The group velocity (v_g) of PAWs is obtained through the compatibility condition as follows:

$$v_g = \frac{-2\, k\omega\, \gamma_1(-\omega^2 + \omega_{c_1}^2)}{(\omega^4 + \omega_{c_1}^4 - 1)k^4 + F_6}, \tag{19}$$

and the coefficients F_{1-6} are given in the appendix. At the same order (second-order), with $s = 2$ and $q = 2$, the harmonic is found to be proportional to $|n_1^{(1)}|^2$:

$$\begin{aligned} &(k^2 + \gamma_1)^2 n_2^{(2)} - (4\, k^2 + \gamma_1)\, (k^2 + \gamma_1)^2\, \Phi_2^{(2)} - |n_1^{(1)}|^2\, \gamma_2 = 0, \\ &-2\,\mathrm{i}\omega\, (k^2 + \gamma_1)^2 (\omega - \omega_{c_1})^2 (\omega + \omega_{c_1})^2 v_2^{(2)} \\ &+|n_1^{(1)}|^2\, \omega_{c_1} k^3 \omega \\ &+\omega_{c_1} (\omega - \omega_{c_1})^2 (\omega + \omega_{c_1})^2 (k^2 + \gamma_1)^2 u_2^{(2)} = 0, \\ &-\omega_{c_1} (\omega - \omega_{c_1})^2 (\omega + \omega_{c_1})^2 (k^2 + \gamma_1)^2 v_2^{(2)} \\ &-2\,\mathrm{i}\omega\, (k^2 + \gamma_1)^2 (\omega - \omega_{c_1})^2 (\omega + \omega_{c_1})^2 u_2^{(2)} \\ &+2\,\mathrm{i}\, k\, (k^2 + \gamma_1)^2 (\omega + \omega_{c_1})^2 (\omega - \omega_{c_1})^2\, \Phi_2^{(2)} \\ &+\mathrm{i}|n_1^{(1)}|^2\, k^3 \omega^2 = 0, \end{aligned} \tag{20}$$

and thus, the corresponding solutions read:

$$\begin{aligned} \Phi_2^{(2)} &= C_6\, |n_1^{(1)}|^2, \qquad n_2^{(2)} = C_4\, |n_1^{(1)}|^2, \\ u_2^{(2)} &= C_5\, |n_1^{(1)}|^2, \qquad v_2^{(2)} = C_7\, |n_1^{(1)}|^2, \end{aligned} \tag{21}$$

and the coefficients C_{4-7} are given in the appendix.

Combining the second-order harmonic with $s = 2$ and $q = 0$ and the third-order equations, one can obtain the

following system:

$$
\begin{aligned}
&k^2(k^2+2\,\gamma_1)n_0^{(2)}-k^2\gamma_1\,(k^2+2\,\gamma_1)\,\Phi_0^{(2)}-2\;|n_1^{(1)}|^2=0,\\
&(-v_{\rm g}k^2\,(\omega-\omega_{c_1})^2\,(\omega+\omega_{c_1})^2\,(k^2+2\,\gamma_1)-(\omega-\omega_{c_1})^2\,(\omega+\omega_{c_1})^2\,v_{\rm g}\gamma_1{}^2)\,\frac{\partial}{\partial\xi}n_0^{(2)}\\
&+(((k^2+\gamma_1)\,\omega^2-\omega_{c_1}^2(k^2+2\,\gamma_1))((k^2+\gamma_1)\,\omega^2-k^2\omega_{c_1}^2)+\gamma_1{}^2\omega_{c_1}^2)\,\frac{\partial}{\partial\eta}v_0^{(2)}\\
&+(\omega-\omega_{c_1})^2(\omega+\omega_{c_1})^2(k^2+\gamma_1)^2\,\frac{\partial}{\partial\xi}u_0^{(2)}+2\,k\omega\,(k^2+\gamma_1)(\omega^2-\omega_{c_1}^2)\,\frac{\partial}{\partial\xi}\,|n_1^{(1)}|^2\\
&-2\,{\rm i}(k^2+\gamma_1)k\omega_{c_1}(\omega^2-\omega_{c_1}^2)\,\frac{\partial}{\partial\eta}\,|n_1^{(1)}|^2=0,\\
&((k^2+\gamma_1)^3\omega_{c_1}^6-3\,(3\,k^2\gamma_1{}^2+\gamma_1{}^3+(-3\,k^4\omega^2\\
&+3\,k^4)\gamma_1+k^6)\omega^2\omega_{c_1}^4+3\,\omega^4(k^6+3\,k^2\gamma_1{}^2+\gamma_1{}^3)\,\omega_{c_1}^2-\omega^6(k^2+\gamma_1)^3)\,\frac{\partial}{\partial\xi}\Phi_0^{(2)}\\
&+v_{\rm g}(\omega-\omega_{c_1})^3(\omega+\omega_{c_1})^3(k^2+\gamma_1)^3\frac{\partial}{\partial\xi}u_0^{(2)}-k^2\omega^2(k^2+\gamma_1)(\omega^2-\omega_{c_1}^2)\frac{\partial}{\partial\xi}\,|n_1^{(1)}|^2\\
&+{\rm i}(k^2+\gamma_1)\omega\,\omega_{c_1}k^2(\omega^2-\omega_{c_1}^2)\,\frac{\partial}{\partial\eta}\,|n_1^{(1)}|^2=0,\\
&-(\omega-\omega_{c_1})^3(\omega+\omega_{c_1})^3(k^2+\gamma_1)^3\frac{\partial}{\partial\eta}\Phi_0^{(2)}+v_{\rm g}(\omega-\omega_{c_1})^3(\omega+\omega_{c_1})^3(k^2+\gamma_1)^3\frac{\partial}{\partial\xi}v_0^{(2)}\\
&-{\rm i}(kv_{\rm g}-\omega)(k^2+\gamma_1)\omega_{c_1}k^2(\omega^2-\omega_{c_1}^2)\,\frac{\partial}{\partial\xi}\,|n_1^{(1)}|^2\\
&-k^2(\omega^2-2\,\omega_{c_1}^2)(k^2+\gamma_1)\,(\omega^2-\omega_{c_1}^2)\,\frac{\partial}{\partial\eta}\,|n_1^{(1)}|^2=0.
\end{aligned}
\tag{22}
$$

Solving system (22) and using the above solutions leads to the following amplitude equation:

$$
\begin{aligned}
&\delta_1\frac{\partial^2}{\partial\xi^2}n_0^{(2)}-\frac{\partial^2}{\partial\eta^2}n_0^{(2)}\\
&\quad-\delta_2\frac{\partial^2}{\partial\xi^2}\,|n_1^{(1)}|^2-\delta_3\frac{\partial^2}{\partial\eta^2}\,|n_1^{(1)}|^2=0,
\end{aligned}
\tag{23}
$$

with the coefficients,

$$
\begin{aligned}
&\delta_1=\gamma_1{v_{\rm g}}^2-1,\\
&\delta_2=\frac{k^2(2\,v_{\rm g}k^3\omega\,\gamma_1(k^2+2\,\gamma_1)+F_7-2\,k^2\gamma_2)}{(k^2+\gamma_1)^4(-\omega^2+\omega_{c_1}^2)^2},\\
&\delta_3=-\frac{k^2(\omega_{c_1}^2\gamma_1(k^2+\gamma_1)^2-k^2\gamma_1(k^2+\gamma_1)-2\,k^2\gamma_2)}{(k^2+\gamma_1)^4(-\omega^2+\omega_{c_1}^2)^2}.
\end{aligned}
\tag{24}
$$

Applying the same method to the third-order algebraic equations and simultaneously using the above solutions and equations, one can obtain the second equation of the DS system:

$$
\begin{aligned}
&{\rm i}\frac{\partial}{\partial\tau}n_1^{(1)}+\lambda_1\frac{\partial^2}{\partial\xi^2}n_1^{(1)}+\lambda_2\frac{\partial^2}{\partial\eta^2}n_1^{(1)}\\
&\quad+\lambda_3\,|n_1^{(1)}|^2n_1^{(1)}+\lambda_4n_0^{(2)}n_1^{(1)}=0,
\end{aligned}
\tag{25}
$$

with their corresponding coefficients as:

$$
\begin{aligned}
&\lambda_1=-\frac{(\omega_{c_1}^2(k^2+\gamma_1)(3\,k^2-\gamma_1)+3\,k^4)\omega\,\gamma_1}{2\,(k^2+\gamma_1)^2(\omega_{c_1}^2k^2+\omega_{c_1}^2\gamma_1+k^2)^2},\\
&\lambda_2=\frac{\omega\,\gamma_1}{2\,(k^2+\gamma_1)(k^2+\omega_{c_1}^2(k^2+\gamma_1))},\\
&\lambda_3=-\frac{\omega\,(A\omega_{c_1}^4+B\omega_{c_1}^2+C)}{F_8\,(k^2+\gamma_1)((4\,k^4+5\,k^2\gamma_1+\gamma_1{}^2)\omega_{c_1}^2+4\,k^4)},\\
&\lambda_4=-\frac{\omega\,k^2(\gamma_1(k^2+\gamma_1)-2\,\gamma_2)}{2\,(k^2+\gamma_1)\gamma_1(k^2+\omega_{c_1}^2(k^2+\gamma_1))},
\end{aligned}
\tag{26}
$$

and the coefficients F_7, F_8, A, B and C are given in the appendix. Equations (23) and (25) are called DS equations in (2+1)-dimensional form, which were first obtained by Davey and Stewartson to show the behavior of a modulated wave train in shallow water [59].

4. Modulational instability analysis

The emergence of modulated waves, such as solitons, is strongly dependent on the stability criteria. Thereby, in this section, we are going to look for the (in)stability conditions of PAWs, according to the DS equations. We set $H=n_1^{(1)}$ and $S=n_0^{(2)}$, and then equations (23) and (25) become:

$$
{\rm i}\frac{\partial H}{\partial\tau}+\lambda_1\frac{\partial^2H}{\partial\xi^2}+\lambda_2\,\frac{\partial^2H}{\partial\eta^2}+\lambda_3\,|H|^2\,H+\lambda_4S\,H=0,
\tag{27}
$$

$$
\delta_1\frac{\partial^2S}{\partial\xi^2}-\frac{\partial^2S}{\partial\eta^2}-\delta_2\frac{\partial^2|H|^2}{\partial\xi^2}-\delta_3\frac{\partial^2|H|^2}{\partial\eta^2}=0.
\tag{28}
$$

In this section, we are going to look after the MI of a plane wave solution of equations (27) and (28). These equations have trivial homogeneous solutions in the form:

$$
\begin{aligned}
H&=H_0{\rm e}^{{\rm i}(-\varpi\,\tau+a_2\eta+a_1\xi+\varphi)},\\
S&=S_0,
\end{aligned}
\tag{29}
$$

where the dispersion relation reads:

$$
\varpi=-\lambda_3H_0^2+\lambda_1a_1{}^2+\lambda_2a_2^2-\lambda_4S_0.
\tag{30}
$$

Furthermore, we insert small perturbations in both the amplitude and phase to perform the stability of the system.

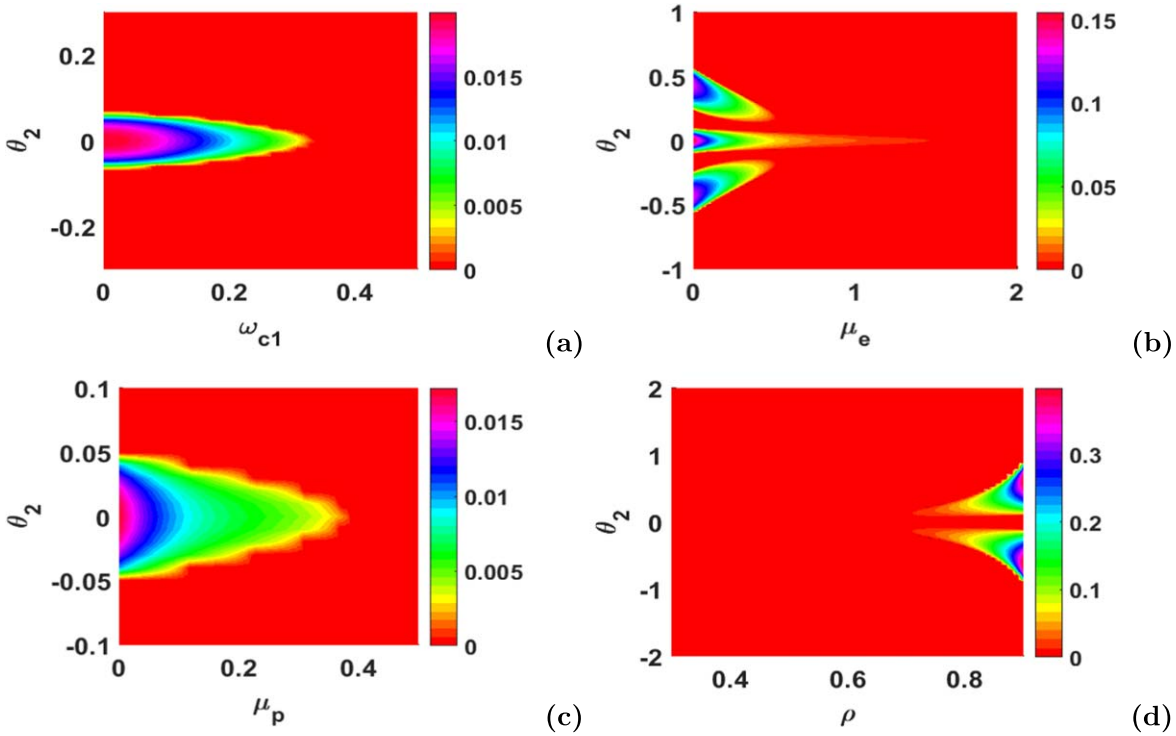

Figure 1. Growth rate of MI is plotted against θ_2 and the other physical parameters: (a) (ω_{c_1}, θ_2), (b) (μ_e, θ_2), (c) (μ_p, θ_2) and (d) (ρ, θ_2). Here, $\mu_e = 1.5$, $\omega_{c_1} = 0.3$, $\rho = 0.5$, $\theta_1 = 0.1$, $\mu_p = 0.3$ and $\sigma = 2$.

$$H = (H_0 + \Delta H)e^{i(-\varpi\,\tau + a_2\eta + a_1\xi + \Delta\varphi + \varphi)},$$
$$S = S_0 + \Delta S. \tag{31}$$

Thus, the perturbed solutions are assumed to be:

$$\begin{bmatrix}\Delta H\\ \Delta S\\ \Delta\varphi\end{bmatrix} = \begin{bmatrix}\delta H\\ \delta S\\ \delta\varphi\end{bmatrix} \mathrm{Re}\,(e^{i(-\Omega\,\tau + \theta_2\eta + \theta_1\xi)}), \tag{32}$$

where $\theta_{1,2}$ are the perturbed wavenumbers. Using all the assumptions above and after a whole mathematical calculation, the nonlinear dispersion relation is obtained as:

$$\Omega^2 = (\lambda_1\theta_1^2 + \lambda_2\theta_2^2)^2\left(1 + \frac{2\,H_0^2\left(\frac{\lambda_4(\delta_2\theta_1^2 + \delta_3\theta_2^2)}{-\delta_1\theta_1^2 + \theta_2^2} - \lambda_3\right)}{\lambda_1\theta_1^2 + \lambda_2\theta_2^2}\right). \tag{33}$$

According to the instability condition ($\Omega^2 < 0$), the threshold amplitude reads:

$$H_{0,\mathrm{cr}}^2 = \frac{(\lambda_1\theta_1^2 + \lambda_2\theta_2^2)(-\delta_1\theta_1^2 + \theta_2^2)}{-2\,\delta_1\theta_1^2 + 2\,\theta_2^2 - 2\,\lambda_4(\delta_2\theta_1^2 + \delta_3\theta_2^2)}. \tag{34}$$

If $\Omega^2 > 0$, the perturbed frequency is real and the system is stable. On the other hand, if $\Omega^2 < 0$, the perturbed frequency becomes imaginary and the system develops an instability. The MI growth rate generally takes the form $\Gamma = \sqrt{-\Omega^2}$. Thus, figure 1 displays the growth rate of MI with different plasma parameters versus the wavenumber θ_2. The red color indicates the stable region whereas the other colors show the unstable region. In the (ω_{c_1}, θ_2) plane (see figure 1(a)), a single lobe of instability is observed and the maximum MI gain decreases with the increase in the MF parameter. Therefore, modulated PAWs become stable for higher values of ω_{c_1}. This behavior is also observed in the (μ_e, θ_2) plane (see figure 1(b)) and (μ_p, θ_2) plane (see figure 1 (c)). However, in the case of figure 1(b), the MI gain displays three lobes of instability. One can see in figure 1(d), which displays the MI gain in the (ρ, θ_2) plane, that the maximum growth rate occurs at higher values of the nonthermal parameter and the instability tends to disappear at lower values of ρ, i.e. when positrons obey Maxwellian distribution.

Figure 2 displays the MI gain versus the wavenumber θ_1 with variations in the MF parameter ω_{c_1} (figure 2(a)), the density ratio of hot electron and cold positron μ_e (figure 2(b)), the density ratio of cold positron and hot positron μ_p (figure 2(c)), and nonthermal parameter ρ (figure 2(d)). One observes here two lobes of instability that are symmetric with respect to the line $\theta_1 = 0$ and the maximum MI gain decreases with the increase in the above plasma parameters. When the MF parameter ω_{c_1} and the density ratio of cold positron and hot positron μ_p increase, the MI gain is shifted towards higher values of the wavenumber θ_1, as shown in panels (a) and (c) of figure 2, respectively. However, in the (μ_e, θ_2) plane (see figure 2(b)), the MI gain is bounded. In these previous cases, the system is stable for the higher values of different plasma parameters. This is different from the case obtained in figure 2(d) where there is no MI gain both for the lower and higher values of the nonthermal parameter. The MI appears only for the finite values of the nonthermal parameter.

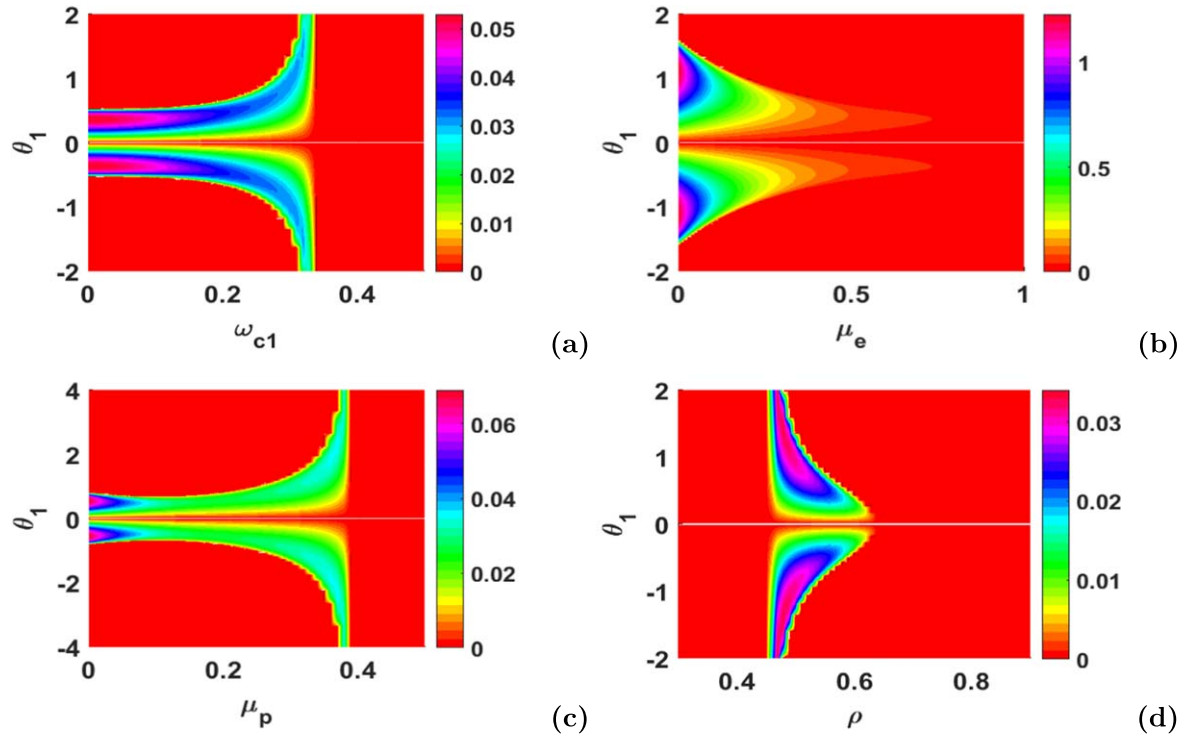

Figure 2. Growth rate of MI is plotted against θ_1 and the other physical parameters: (a) (ω_{c_1}, θ_1), (b) (μ_e, θ_1), (c) (μ_p, θ_1), (d) (ρ, θ_1). Here, $\mu_e = 1.5$, $\omega_{c_1} = 0.3$, $\rho = 0.5$, $\mu_p = 0.3$ and $\sigma = 2$.

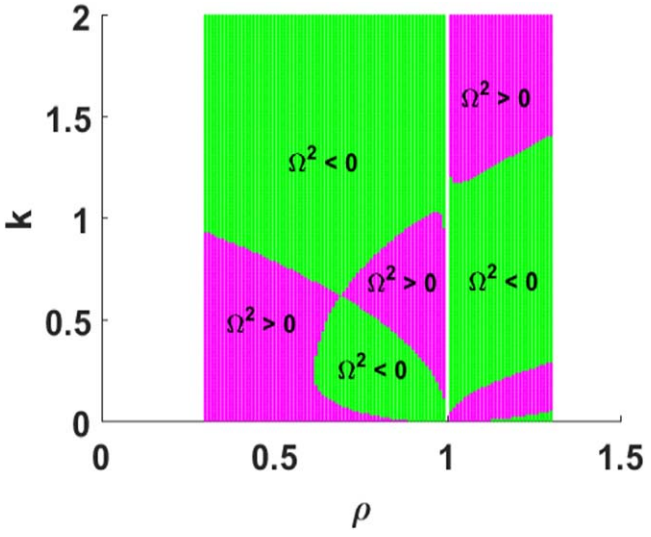

Figure 3. Diagram of stability/instability versus rho, with $\mu_e = 1.5$, $\mu_p = 0.3$, $\omega_{c_1} = 0.3$, $\rho = 0.5$ and $\sigma = 2$.

According to equation (33), we can approximate the stability condition through the following function:

$$g(\rho, k) = (\lambda_1 + \lambda_2)\left(-\lambda_3 + \frac{\lambda_4(\delta_2 + \delta_3)}{1 - \delta_1}\right). \tag{35}$$

Then, the stability/instability diagram of parameters ρ and k is plotted in figure 3, which shows the region where the localized structures, such as dromion solitons, appear. This figure shows that the stability/instability zone is very sensitive to the non-thermal parameter. This can help us to choose the appropriate values of parameters k and ρ for which the dromion solitons emerge. The localized structures are generally observed in the unstable region of MI, i.e $\Omega^2 < 0$. However, all the values of the parameters (k, ρ) that fall inside the green region can lead to the formation of the dromion solitons.

Previous MI studies regarding PAWs have only been done in the (1+1) dimension, and the MI in the (2+1)-dimension differs from the (1+1) dimension, both qualitatively and quantitatively. The MI growth rate of PAWs in the (1+1) dimension depends on the product of the coefficients of nonlinear and dispersive terms [3], which are the functions of the physical parameters involved. If the product is positive, the amplitude-modulated envelope is unstable for perturbation wavelengths larger than a critical value, hence the carrier wave leads to the formation of a bright soliton. On the other hand, if the product is negative, the amplitude-modulated envelope will be stable against external perturbations and may propagate in the form of a dark soliton. Moreover, the stability zone is very well separated from the instability zone. From our plasma model of (2+1) PAW, we noticed that the growth rate and instability condition is more complicated, involving longitudinal and transverse components through θ_1 and θ_2, respectively. In addition, the (in)stability diagram obtained in our study is more complex and we observed an alternation between the stability and instability zones, as demonstrated by figure 3.

5. Dromion structure

In this section, we look for a particular kind of soliton solution of equations (27) and (28) called the dromion soliton.

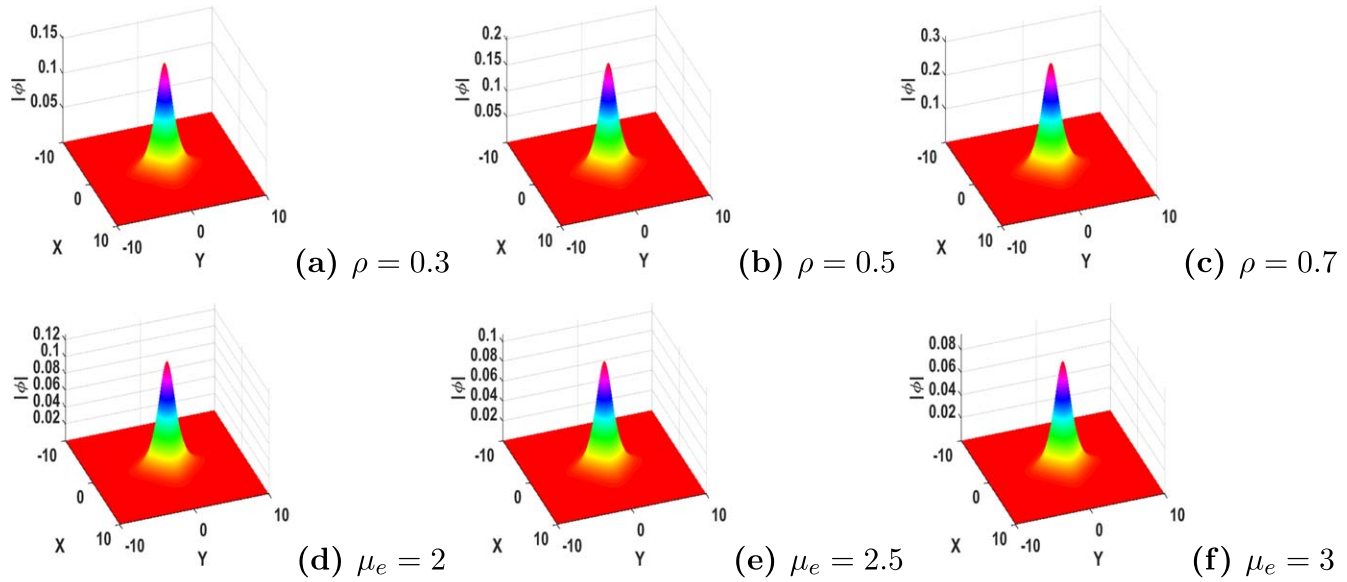

Figure 4. Plots of one-dromion solitons are plotted in the (x, y)-plane and for different values of (ρ, μ_e): (a) (ρ, μ_e)=(0.3, 1.5), (b) (ρ, μ_e)=(0.5, 1.5), (c) (ρ, μ_e)=(0.7, 1.5), (d) (ρ, μ_e)=(0.5, 2), (e) (ρ, μ_e)=(0.5, 2.5), (f) (ρ, μ_e)=(0.5, 3). Here, $\mu_p = 0.3$, $\omega_{c_1} = 0.3$, $\sigma = 2$, $t = 0$, $h_1 = 1$, $r_1 = r_2 = b_1 = 1$ and $(\chi_i)_{i=1,2,3} = 1$.

However, it is necessary to convert these equations into standard DS ones. Furthermore, by introducing a new dependent variable (ζ, ς) and pivoting from 0 to $\frac{\pi}{4}$ the coordinate axis, we obtain [48]:

$$\zeta = \frac{\xi}{\sqrt{\delta_1\lambda_3 + \delta_2\lambda_4}}, \qquad \varsigma = \frac{\eta}{\sqrt{-\delta_3\lambda_4 + \lambda_3}},$$
$$X = \frac{(\zeta + \varsigma)}{\sqrt{2}}, \qquad Y = \frac{(\zeta - \varsigma)}{\sqrt{2}}. \tag{36}$$

$$\mathrm{i}H_\tau + a(H_{XX} + H_{YY}) + bH_{YY} + d\,S\,H + c\,|H|^2 H = 0, \tag{37}$$

$$e(S_{XX} + S_{YY}) + fS_{XY} + 2(|H|)^2_{XY} = 0, \tag{38}$$

where

$$a = \frac{\lambda_1}{2\,\delta_1\lambda_3 + 2\,\delta_2\lambda_4} + \frac{\lambda_2}{-2\,\delta_3\lambda_4 + 2\,\lambda_2},$$
$$b = \frac{\lambda_1}{2\,\delta_1\lambda_3 + 2\,\delta_2\lambda_4} - \frac{\lambda_2}{-2\,\delta_3\lambda_4 + 2\,\lambda_2},$$
$$c = \lambda_3, \quad d = \lambda_4,$$
$$e = \frac{\delta_1}{2\,\delta_1\lambda_3 + 2\,\delta_2\lambda_4} - \frac{1}{(-2\,\delta_3\lambda_4 + 2\,\lambda_2)},$$
$$f = \frac{\delta_1}{2\,\delta_1\lambda_3 + 2\,\delta_2\lambda_4} + \frac{1}{(-2\,\delta_3\lambda_4 + 2\,\lambda_2)}. \tag{39}$$

Now, we transform them into the bilinear form by assuming that $H = \frac{G}{F}$ and $S = c\,(\ln \mathrm{H})_{XY}$. Then, the bilinear form of equations (37) and (38) reads:

$$[\mathrm{i}\,D_\tau + a\,(D_{XX} + D_{yy}) + b\,D_{XY}]G.H = 0,\ D_{XY}\,H.H = m\,G.G^*, \tag{40}$$

where $F = 1 + \varepsilon^2 f_2 + \varepsilon^4 f_4$ and $G = \varepsilon\, g_1 + \varepsilon^3\, g_3$. However, according to the Hirota method [60–69] the expressions of f_2, f_4, g_1 and g_3 can be easily found. Then, the single dromion solution of DS equations (37) and (38) reads:

$$H_1 = \frac{h_1 \mathrm{e}^{\vartheta_1 + \vartheta_2}}{1 + \chi_1 \mathrm{e}^{\vartheta_1^* + \vartheta_1} + \chi_2 \mathrm{e}^{\vartheta_2^* + \vartheta_2} + \chi_3 \mathrm{e}^{\vartheta_1^* + \vartheta_2^* + \vartheta_1 + \vartheta_2}}, \tag{41}$$

with the quantities:

$$\vartheta_1 = \mathrm{i}\omega_1 t + r_1 X + b_1,$$
$$\vartheta_2 = \mathrm{i}\omega_2 t + r_2 Y + b_2. \tag{42}$$

Here, ϑ^* is the conjugate of ϑ, $\omega_1 = \mathrm{i}\,a\,r_1^2$ and $\omega_2 = \mathrm{i}\,a\,r_2^2$, along with h_1, $(\chi_i)_{i=1,2,3}$ and $(r_i)_{i=1,2}$ are all the real constants. By a similar procedure, the two-dromion solution of DS is given as:

$$H_2 = \frac{l_1 \mathrm{e}^{\vartheta_1 + \vartheta_3} + l_2 \mathrm{e}^{\vartheta_2 + \vartheta_3} + l_3 \mathrm{e}^{\vartheta_1^* + \vartheta_1 + \vartheta_2 + \vartheta_3} + l_4 \mathrm{e}^{\vartheta_2^* + \vartheta_1 + \vartheta_2 + \vartheta_3}}{\Gamma_1 + \Gamma_2 + \Gamma_3}, \tag{43}$$

with

$$\Gamma_1 = 1 + L_1 \mathrm{e}^{\vartheta_1^* + \vartheta_1} + L_2 \mathrm{e}^{\vartheta_2^* + \vartheta_2} + L_3 \mathrm{e}^{\vartheta_3^* + \vartheta_3} + L_4(\mathrm{e}^{\vartheta_2^* + \vartheta_1} + \mathrm{e}^{\vartheta_1^* + \vartheta_2}),$$
$$\Gamma_2 = L_5(\mathrm{e}^{\vartheta_2^* + \vartheta_3^* + \vartheta_1 + \vartheta_3} + \mathrm{e}^{\vartheta_1^* + \vartheta_3^* + \vartheta_2 + \vartheta_3}) + L_6 \mathrm{e}^{\vartheta_1^* + \vartheta_2^2 + \vartheta_1 + \vartheta_2},$$
$$\Gamma_3 = L_7 \mathrm{e}^{\vartheta_2^* + \vartheta_3^* + \vartheta_2 + \vartheta_3} + L_8 \mathrm{e}^{\vartheta_1^* + \vartheta_3^* + \vartheta_1 + \vartheta_3} + L_9 \mathrm{e}^{\vartheta_1^* + \vartheta_2^* + \vartheta_3^* + \vartheta_1 + \vartheta_2 + \vartheta_3}, \tag{44}$$

where $(l_i)_{i=1,2,3,4}$, $(L_i)_{i=1-9}$, $(b_i)_{i=1,2,3}$ and $(r_i)_{i=1,2,3}$ are all the real constants:

$$\vartheta_1 = \mathrm{i}\omega_1 t + r_1 X + b_1,$$
$$\vartheta_2 = \mathrm{i}\omega_2 t + r_2 X + b_2,$$
$$\vartheta_3 = \mathrm{i}\omega_3 t + r_3 Y + b_3. \tag{45}$$

The one-dromion soliton is depicted in figure 4, which shows the impact of the nonthermal parameter ρ and the ratio of hot electron to cold positron μ_e. The impact of ρ on the amplitude of this wave is shown in figures 4(a–c) and one can see that the amplitude of the one-dromion soliton increases with the increase in the value of ρ. Thus, increasing the nonthermal parameter would lead to an enhancement in the energy in the system, which causes an increase in nonlinearity. Therefore, the amplitude becomes larger, indicating that the nonthermal parameter is pumping more energy towards the background waves, which are sucked in to create the acoustic positron waves. The response of the one-dromion soliton due to μ_e is shown in figures 4(d–f). Here, one can

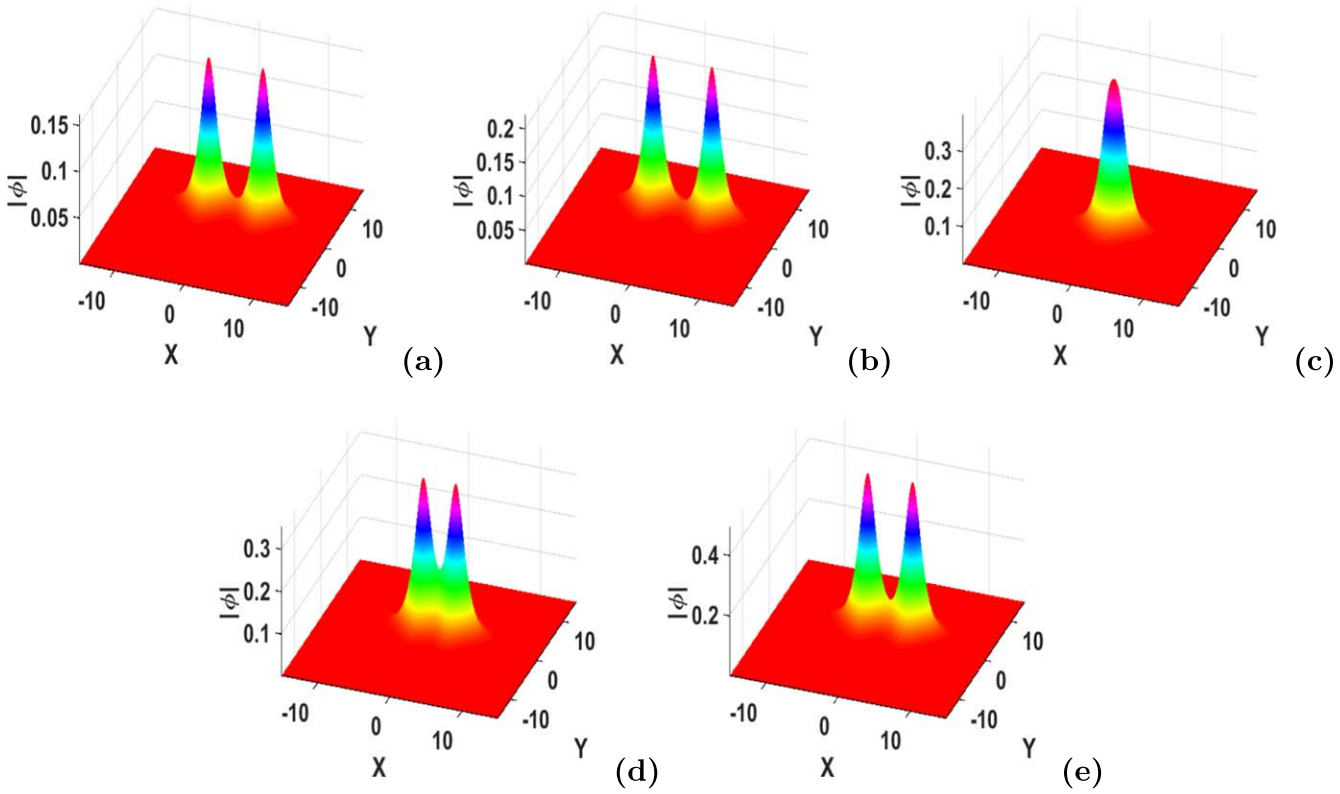

Figure 5. Profile of elastic collision between two dromion solitons is plotted against ρ: (a) $\rho = 0.3$, (b) $\rho = 0.5$, (c) $\rho = 0.65$, (d) $\rho = 0.7$, (e) (a) $\rho = 0.8$. Here, $\mu_e = 1.5$, $\mu_p = 0.3$, $\omega_{c_1} = 0.3$, $t = 8$, $\rho = 0.5$, $(l_i)_{i=1,2,3,4} = 1$, $(L_i)_{i=1-9} = 1$, $b_1 = b_3 = 1$, $b_2 = 2$, $r_1 = r_3 = 1$, $r_2 = -1$ and $\sigma = 2$.

observe that the amplitude of this wave drops with the increase in the value of μ_e. Certainly, increasing μ_e diminishes the nonlinearity of the system, and consequently diminishes the amplitude of the wave.

A comparison of the above results with those of (1+1)-dimensional PAW plasma models is also enlightening. It is interesting to note that the DS equation supports only the compressive (positive) solitons. This behavior is different from that obtained in the 1D case. In the latter case, using a PAW model, compressive (positive) and rarefactive (negative) solitons were studied within the framework of the Korteweg–de Vries equation with emphasis on the effect of the nonthermal parameter [44]. It was found that the nonthermal parameter increases the amplitude and width of the compressive and rarefactive solitary waves.

The interactions of the two dromion solitons are depicted in Figures 5–7. In general, the interactions between two solitons are elastic and inelastic collisions. Figure 5 displays the elastic collision between two dromion solitons at time $t = 8$ due to the effect of the nonthermal parameter (Panel (5a) with $\rho = 0.3$; panel 5(b) with $\rho = 0.5$; panel 5(c) with $\rho = 0.65$; panel 5(d) with $\rho = 0.7$ and panel 5(e) with $\rho = 0.8$). Here, we observe a remarkable effect of the ρ parameter during the interaction between these two solitons. Indeed, when ρ increases, the amplitude of the two waves increases (see figures 5(a), 5(b)). For a particular value of ρ, the two dromions collide to form a single structure (see figure 5(c). As the value of ρ increases, the two dromions dissociate (see figure 5(d)) and gradually move away from each other (see figure 5(e)) with an amplitude gain due to the increase in ρ. In this context, we can confirm that the nonthermal parameter favors the phenomenon of elastic collision between two dromions in a magnetized plasma model where the dynamics of positrons is considered.

Figure 6 illustrates the elastic collision between two dromion solitons at different times. Figure 6(a) displays two dromion solitons that come from far away with equal amplitude at time $t = -10$, and collide at $t = 0$ (see figure 6(b)), then become unique at $t = 3$ with higher amplitude (see figure (6c)). After collision, each soliton keeps its characteristics constant. These kinds of interactions were obtained by Tabi *et al* [49] in electronegative plasma. Figure 7 displays the inelastic collision between two dromion solitons at different times. One can observe from figure 7(a) that, at $t = -10$, two dromion solitons come from far away with different amplitudes and collide (see figure (7b)) at $t = 0$, then become a single dromion at $t = 3$ (see figure (7c)). The remarkable and rare phenomenon observed here is that of energy transfer during the collision. Thus, this phenomenon is justified by the amplitudes of the solitons of figures 7(d), (e) after collision. The tallest has transferred an amount of energy to the shortest. The amplitude of the tallest decreases to compensate for that of the shortest. These elastic and inelastic collision phenomena are observed between energetic particles in confined plasma, during the production of energy by

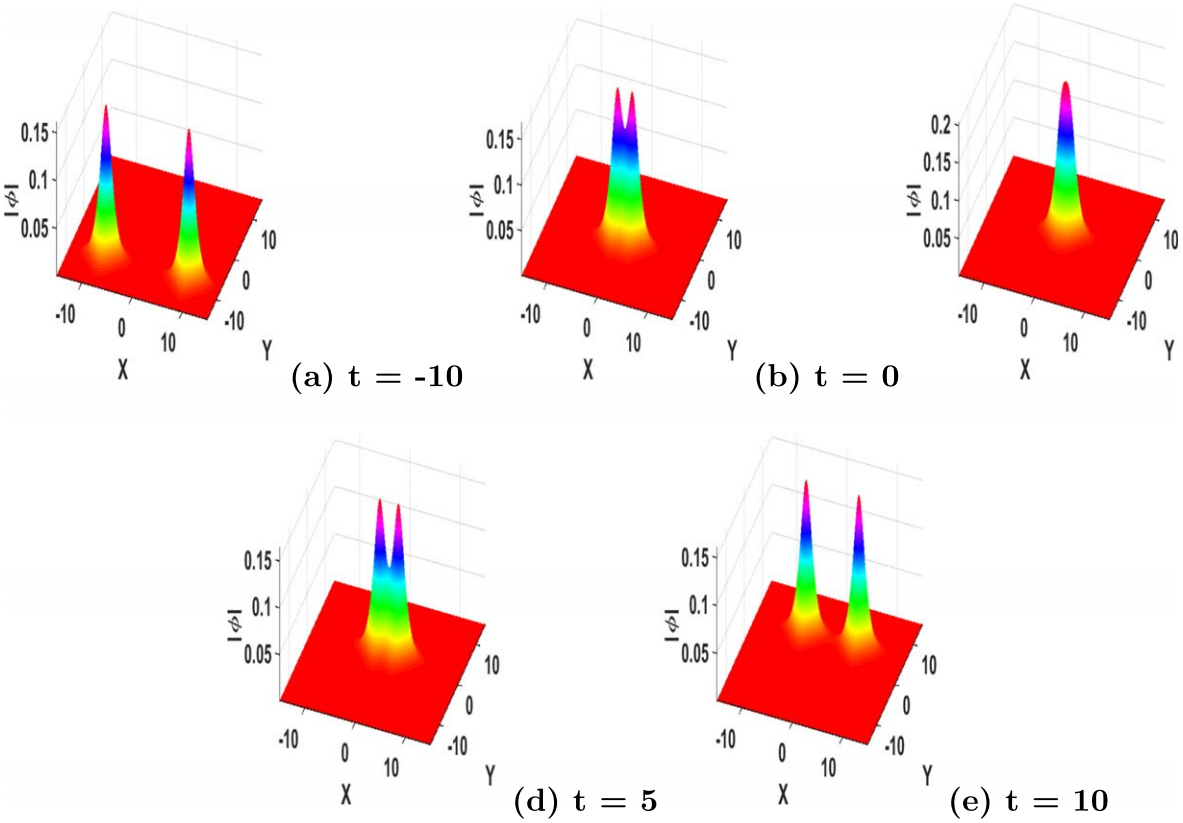

Figure 6. Profile of elastic collision between two dromion solitons is plotted against different values of t: (a) $t=-10$, (b) $t=0$, (c) $t=3$, (d) $t=5$, (e) $t=10$. Here, $\mu_{\mathrm{e}}=1.5$, $\mu_{\mathrm{p}}=0.3$, $\omega_{\mathrm{c_1}}=0.3$, $\rho=0.5$, $\sigma=2$, $(l_i)_{i=1,2,3,4}=1$, $(L_i)_{i=1-9}=1$, $b_1=b_3=1$, $b_2=2$, $r_1=r_3=1$ and $r_2=-1$.

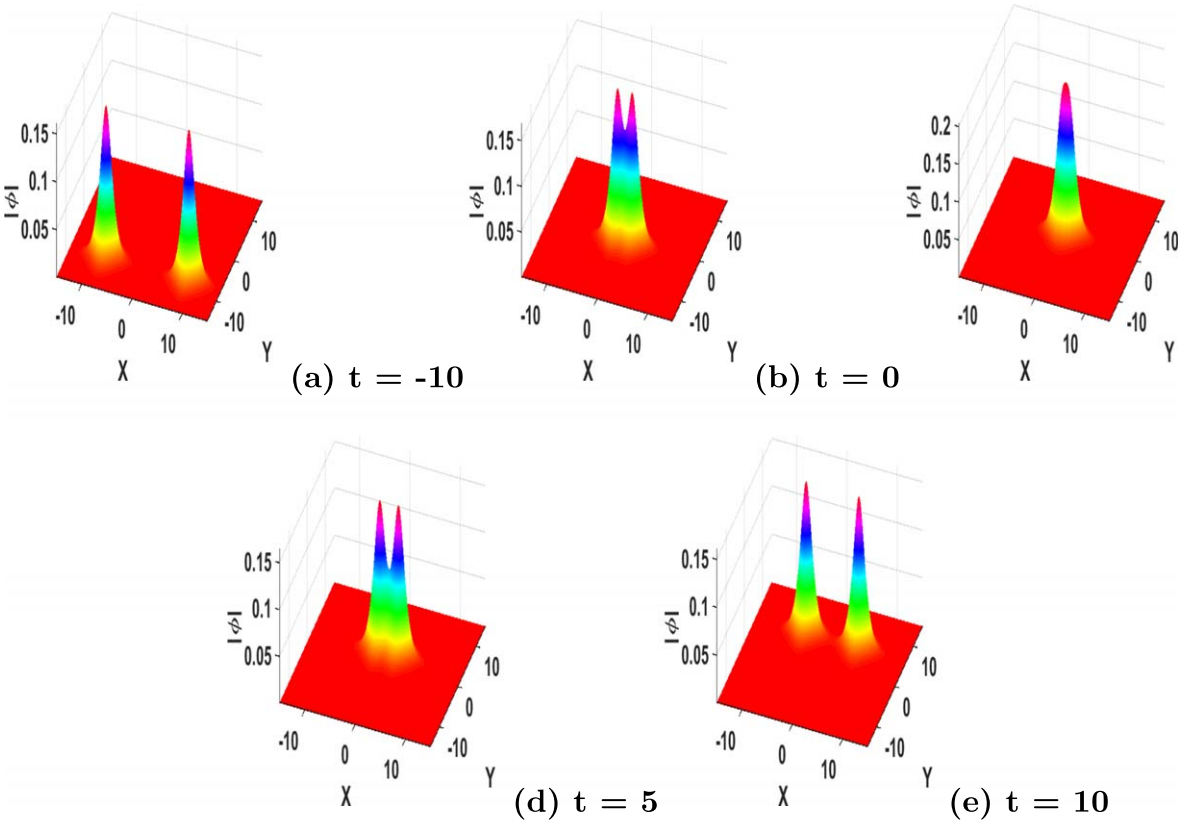

Figure 7. Profile of inelastic collision between two dromion solitons is plotted against different values of t: (a) $t=-10$, (b) $t=0$, (c) $t=3$, (d) $t=5$, (e) $t=10$. Here, $\mu_{\mathrm{e}}=1.5$, $\mu_{\mathrm{p}}=0.3$, $\omega_{\mathrm{c_1}}=0.3$, $\rho=0.5$, $\sigma=2$, $(L_i)_{i=1-9}=1$, $b_1=b_3=1$, $b_2=2$, $r_1=r_3=1$, $r_2=-1$, $(l_i)_{i=1,2,3}=1$ and $l_4=1.5$.

thermonuclear fusion in a magnetized enclosure called a tokamak [70].

6. Conclusion

In this study, we have investigated the MI and OC between dromion structures of the PAWs in magnetized plasma with nonthermal distribution. The (2+1)-dimensional DS equations have been derived according to the standard RPM. Through the stability criteria, we have determined the region where the localized structures, such as dromion solitons, appear. In that respect, a comprehensive analysis of wave instability has been conducted, where regions of stability/instability have been revealed to be very sensitive to the nonthermal parameter, the strength of MF, the density ratio of hot electron and cold positron, and the density ratio of cold positron and hot positron. Using the Hirota method, we have shown that the plasma model supports some exact solutions such as one- and two-dromion solutions. We have discussed the elastic and inelastic collisions between two dromions. We have noticed that the characteristics of dromion solutions are very sensitive to the change of some plasma parameters. In particular, we have shown that the nonthermal parameter favors the phenomenon of elastic collision between two dromions, whereas, during the inelastic collision, the remarkable and rare phenomenon observed here is that of energy transfer during the collision. The relevance of this study is that it can help to explain the main mechanisms leading to the generation of plasma particles, through energy recombination among the available dynamical modes when the positrons and electrons interact. This insight is crucial for advancing our knowledge of plasma physics and for applications such as controlled fusion and astrophysical research.

Acknowledgments

The authors extend their appreciation to the Deanship of Scientific Research and Libraries in Princess Nourah bint Abdulrahman University for funding this research work through the Research Group project under Grant No. (RG-1445-0005).

Conflict of interest

The authors declare that they have no conflicts of interest.

Author contributions

All authors contributed equally and approved the final version of the current manuscript.

Use of AI tools declaration

The authors declare that they have not used artificial intelligence (AI) tools in the creation of this article.

Appendix. Expression of the coefficients

The coefficients of equations (18) and (19) are:

$$\begin{aligned}
F_1 &= v_g k^3\omega^2 + v_g\omega_{c_1}^2 k^3 + k^2\omega^3 - \omega_{c_1}^2 k^2\omega,\\
F_2 &= v_g k\omega^2\gamma_1 + k\gamma_1\omega_{c_1}^2 v_g - \omega^3\gamma_1 + \omega\,\gamma_1\omega_{c_1}^2,\\
F_3 &= k^4\omega^4 - 2\,k^4\omega^2\omega_{c_1}^2 + k^4\omega_{c_1}^4 + 2\,k^2\omega^4\gamma_1 - 4\,k^2\omega^2\gamma_1\omega_{c_1}^2,\\
F_4 &= 2\,k^2\gamma_1\omega_{c_1}^4 + \omega^4{\gamma_1}^2 - 2\,\omega^2{\gamma_1}^2\omega_{c_1}^2 + {\gamma_1}^2\omega_{c_1}^4,\\
F_5 &= 2\,v_g k^3\omega + k^2\omega^2 - \omega_{c_1}^2 k^2 + 2\,v_g k\omega\,\gamma_1 - \omega^2\gamma_1 + \omega_{c_1}^2\gamma_1,\\
F_6 &= (-2\,\omega^4 + 2\,\omega_{c_1}^4)\gamma_1 k^2 + (-\omega^4 + \omega_{c_1}^4){\gamma_1}^2.
\end{aligned} \tag{A1}$$

The coefficients of equation (21) are:

$$\begin{aligned}
C_4 &= -\frac{(F_9 - 5\,\omega_{c_1}^2\omega^2\gamma_1 + \omega_{c_1}^4\gamma_1 + 2\,k^2\omega^2 + \omega_{c_1}^2 k^2)k^2}{(-4\,\omega^2 + \omega_{c_1}^2)(-k^2\omega^2 + \omega_{c_1}^2 k^2 - \omega^2\gamma_1 + \omega_{c_1}^2\gamma_1)^2} - \frac{4C_6k^2}{-4\,\omega^2 + \omega_{c_1}^2},\\
F_9 &= 4\,k^2\omega^4 - 5\,\omega_{c_1}^2 k^2\omega^2 + \omega_{c_1}^4 k^2 + 4\,\omega^4\gamma_1,\\
C_6 &= \frac{4\,k^4\omega^4 - 5\,\omega_{c_1}^2 k^4\omega^2 + \omega_{c_1}^4 k^4 + 4\,k^2\omega^4\gamma_1 - 5\,\omega_{c_1}^2 k^2\omega^2\gamma_1 + \omega_{c_1}^4 k^2\gamma_1}{(k^2+\gamma_1)^2(16\,k^2\omega^2 - 4\,\omega_{c_1}^2 k^2 + 4\,\omega^2\gamma_1 - \gamma_1\omega_{c_1}^2 - 4\,k^2)(-\omega^2 + \omega_{c_1}^2)^2}\\
&\quad + \frac{-4\,\omega^6\gamma_2 + 9\,\omega_{c_1}^2\omega^4\gamma_2 - 6\,\omega_{c_1}^4\omega^2\gamma_2 + \omega_{c_1}^6\gamma_2 + 2\,k^4\omega^2 + \omega_{c_1}^2 k^4}{(k^2+\gamma_1)^2(16\,k^2\omega^2 - 4\,\omega_{c_1}^2 k^2 + 4\,\omega^2\gamma_1 - \gamma_1\omega_{c_1}^2 - 4\,k^2)(-\omega^2 + \omega_{c_1}^2)^2},\\
C_5 &= \frac{-4\,C_6k\omega}{-4\,\omega^2 + \omega_{c_1}^2} + \frac{k^3(2\,\omega^2 + \omega_{c_1}^2)\omega}{(2\,\omega - \omega_{c_1})(2\,\omega + \omega_{c_1})(\omega - \omega_{c_1})^2(\omega + \omega_{c_1})^2(k^2+\gamma_1)^2},\\
C_8 &= \frac{i\omega_{c_1}k(2\,C_6(\omega - \omega_{c_1})^2(\omega + \omega_{c_1})^2(k^2+\gamma_1)^2 + 3\,k^2\omega^2)}{(\omega - \omega_{c_1})^2(\omega + \omega_{c_1})^2(k^2+\gamma_1)^2(-4\,\omega^2 + \omega_{c_1}^2)}.
\end{aligned} \tag{A2}$$

The coefficients of equations (24) and (26) are:

$$\begin{aligned}
F_7 &= \gamma_1((k^2+\gamma_1)^2\omega_{c_1}^2 + 2\,v_g k\omega\,{\gamma_1}^2) + k^2\gamma_1(k^2+\gamma_1),\\
F_8 &= 6\,\gamma_1((k^6 + 3\,k^4\gamma_1 + 3\,k^2{\gamma_1}^2 + {\gamma_1}^3)\omega_{c_1}^2 + k^6 + 2\,k^4\gamma_1 + k^2{\gamma_1}^2),\\
A &= 24\,k^{12}\gamma_1 + 126\,k^{10}{\gamma_1}^2 + 270\,k^8{\gamma_1}^3 + 300\,k^6{\gamma_1}^4 + 180\,k^4{\gamma_1}^5 + 54\,k^2{\gamma_1}^6 + 6\,{\gamma_1}^7,\\
B &= 72\,k^{12}\gamma_1 + 306\,k^{10}{\gamma_1}^2 + 504\,k^8{\gamma_1}^3 - 16\,k^8\gamma_1\gamma_2 + 396\,k^6{\gamma_1}^4 - 48\,k^6{\gamma_1}^2\gamma_2\\
&\quad + 144\,k^4{\gamma_1}^5 - 36\,k^6\gamma_1\gamma_3 + 48\,k^6{\gamma_2}^2 - 48\,k^4{\gamma_1}^3\gamma_2 + 18\,k^2{\gamma_1}^6 - 45\,k^4{\gamma_1}^2\gamma_3 + 66\,k^4\gamma_1{\gamma_2}^2\\
&\quad - 16\,k^2{\gamma_1}^4\gamma_2 - 9\,k^2{\gamma_1}^3\gamma_3 + 18\,k^2{\gamma_1}^2{\gamma_2}^2,\\
C &= 48\,k^{12}\gamma_1 + 162\,k^{10}{\gamma_1}^2 + 198\,k^8{\gamma_1}^3 - 24\,k^8\gamma_1\gamma_2 + 102\,k^6{\gamma_1}^4 - 48\,k^6{\gamma_1}^2\gamma_2 + 18\,k^4{\gamma_1}^5\\
&= -36\,k^6\gamma_1\gamma_3 + 48\,k^6{\gamma_2}^2 - 24\,k^4{\gamma_1}^3\gamma_2 + 8\,k^4\gamma_1{\gamma_2}^2.
\end{aligned} \tag{A3}$$

References

[1] Saha A 2017 Nonlinear excitations for the positron acoustic shock waves in dissipative nonextensive electron-positron-ion plasmas *Phys. Plasmas* **24** 034502

[2] Mouhammadoul B B, Alim A, Tiofack C G L, Mohamadou A, Alrowaily A W, Ismaeel S M E and El-Tantawy S A 2023 On the super positron-acoustic rogue waves in q-nonextensive magnetoplasmas *Phys. Fluids* **35** 054109

[3] Mouhammadoul B B, Alim, Tiofack C G L and Mohamadou A 2020 Modulated positron-acoustic waves and rogue waves in a magnetized plasma system with nonthermal electrons and positrons *Astrophys. Space Sci.* **365** 90

[4] Rahman M M, Alam M S and Mamun A A 2015 Cylindrical and spherical positron-acoustic shock waves in nonthermal electron-positron-ion plasmas *Braz. J. Phys.* **45** 314

[5] Shah M G, Hossen M R, Sultana S and Mamun A A 2015 Positron-acoustic shock waves in a degenerate multi-component plasma *Chin. Phys. Lett.* **32** 085203

[6] Rahman M M, Alam M S and Mamun A A 2014 Cylindrical and spherical positron-acoustic Gardner solitons in electron-positron-ion plasmas with nonthermal electrons and positrons *Astrophys. Space Sci.* **352** 193

[7] Rahman M M, Alam M S and Mamun A A 2014 Positron-acoustic Gardner solitons and double layers in electron-positron-ion plasmas with nonthermal electrons and positrons *Eur. Phys. J. Plus* **129** 84

[8] Uddin M J, Alam M S and Mamun A A 2015 Nonplanar positron-acoustic Gardner solitary waves in electron-positron-ion plasmas with superthermal electrons and positrons *Phys. Plasmas* **22** 022111

[9] Uddin M J, Alam M S, Masud M M, Anowar G M and Mamun A A 2015 Instability analysis of obliquely propagating positron-acoustic solitary waves in superthermal plasmas *IEEE Trans. Plasma Sci.* **43** 985

[10] Shah M G, Hossen M R and Mamun A A 2015 Nonplanar positron-acoustic shock waves in astrophysical plasmas *Braz. J. Phys.* **45** 219

[11] Tribeche M, Aoutou K, Younsi S and Amour R 2009 Nonlinear positron acoustic solitary waves *Phys. Plasmas* **16** 072103

[12] Sahu B 2010 Positron acoustic shock waves in planar and nonplanar geometry *Phys. Scr.* **82** 065504

[13] Saha A, Ali R and Chatterjee P 2017 Nonlinear excitations for the positron acoustic waves in auroral acceleration regions *Adv. Space Res.* **60** 1220

[14] Saha A and Tamang J 2017 Qualitative analysis of the positron-acoustic waves in electron-positron-ion plasmas with κ deformed Kaniadakis distributed electrons and hot positrons *Phys. Plasmas* **24** 082101

[15] Ali R, Saha A and Chatterjee P 2017 Dynamics of the positron acoustic waves in electron-positron-ion magnetoplasmas *Indian J. Phys.* **91** 689

[16] Popel S I, Golub A P and Losseva T V 2003 Weakly dissipative dust-ion-acoustic solitons *Phys. Rev. E* **67** 056402

[17] Nakamura Y and Sarma A 2001 Observation of ion-acoustic solitary waves in a dusty plasma *Phys. Plasmas* **8** 3921

[18] Yang X, Wang C L, Liu C B, Zhang J R and Shi Y R 2012 The collision effect between dust grains and ions to the dust ion acoustic waves in a dusty plasma *Phys. Plasmas* **19** 103705

[19] Misra A P, Choudhury A R and Choudhury K R 2004 Electrostatic acoustic modes in a self-gravitating complex plasma with variable charge impurities *Phys. Lett.* A **323** 110

[20] El-Tantawy S A, Moslem W M, Sabry R, El-Labany S K, El-Metwally M and Schlickeiser R 2014 Head-on collision of ion-acoustic solitons in an ultracold neutral plasma *Astrophys. Space Sci.* **350** 175

[21] El-Tantawy S A 2016 Nonlinear dynamics of soliton collisions in electronegative plasmas: The phase shifts of the planar KdV-and mkdV-soliton collisions *Chaos, Solitons Fractals* **93** 162

[22] El-Tantawy S A and Wazwaz A M 2018 Anatomy of modified Korteweg–de Vries equation for studying the modulated envelope structures in non-Maxwellian dusty plasmas: Freak waves and dark soliton collisions *Phys. Plasmas* **25** 092105

[23] Hashmi T, Jahangir R, Masood W, Alotaibi B M, Ismaeel S M E and El-Tantawy S A 2023 Head-on collision of ion-acoustic (modified) Korteweg–de Vries solitons in Saturn's magnetosphere plasmas with two temperature superthermal electrons *Phys. Fluids* **35** 103104

[24] Douanla D V, Tiofack C G L, Alim, Aboubakar M, Mohamadou A, Albalawi W, El-Tantawy S A and El-Sherif L S 2022 Three-dimensional rogue waves and dust-acoustic dark soliton collisions in degenerate ultradense magnetoplasma in the presence of dust pressure anisotropy *Phys. Fluids* **34** 087105

[25] Douanla D V, Tiofack C G L, Alim A, Mohamadou A, Alyousef H A, Ismaeel S and El-Tantawy S A 2023 Dynamics and head-on collisions of multidimensional dust acoustic shock waves in a self-gravitating magnetized electron-depleted dusty plasma *Phys. Fluids* **35** 023103

[26] Wazwaz A M, Alhejaili W and El-Tantawy S A 2023 Analytical study on two new (3+1)-dimensional Painlevé integrable equations: Kink, lump, and multiple soliton solutions in fluid mediums *Phys. Fluids* **35** 093119

[27] Wazwaz A M, Alhejaili W and El-Tantawy S A 2023 Study on extensions of (modified) Korteweg–de Vries equations: Painlevé integrability and multiple soliton solutions in fluid mediums *Phys. Fluids* **35** 093110

[28] Salemah A A, Shahida P, Shahzad M, Anisa Q, Alotaibi B M and El-Tantawy S A 2023 On the propagation of cnoidal wave and overtaking collision of slow shear Alfvén solitons in low collision of slow shear Alfvén solitons in low β magnetized plasmas *Phys. Fluids* **35** 075130

[29] Wazwaz A M, Alyousef H A and El-Tantawy S 2023 An extended Painlevé integrable Kadomtsev–Petviashvili equation with lumps and multiple soliton solutions *Int. J. Numer. Methods Heat Fluid Flow* **33** 2533

[30] Gardner C S, Greener J M, Kruskal M D and Mirie R M 1967 Method for solving the Korteweg–de Vries equation *Phys Rev Lett* **19** 1095

[31] Saha A and Chatterjee P 2014 Propagation and interaction of dust acoustic multi-soliton in dusty plasmas with *q*-nonextensive electrons and ions *Astrophys. Space Sci.* **353** 169

[32] Singh K, Singh G and Saini N S 2022 Periodic kinetic Alfvén waves and overtaking between multi-solitons in nonthermal electron-positron-ion plasma *Chin. J. Phys.* **77** 2060

[33] Sahu B 2013 Propagation of two solitons in electron acoustic waves with superthermal electrons *Europhys. Lett.* **101** 55002

[34] Lavanya C 2022 Propagation and soliton collision of positron acoustic waves in four-component space plasmas *Braz. J. Phys.* **52** 38

[35] Haque Q and Saleem H 2003 Ion acoustic and drift wave vortices in electron-positron-ion plasmas *Phys. Plasmas* **10** 3793

[36] Shah A, Saeed R and M Noaman-Ul-Haq M 2010 Nonplanar converging and diverging shock waves in the presence of thermal ions in electron-positron plasma *Phys. Plasmas* **17** 072307

[37] Akbari-Moghshanjoughi M 2010 Effects of ion-temperature on propagation of the large-amplitude ion-acoustic solitons in degenerate electron-positron-ion plasmas *Phys. Plasmas* **17** 082315

[38] El-Awady E I, El-Tantawy S A, Moslem W M and Shukla P K 2010 Electron-positron-ion plasma with kappa distribution: Ion acoustic soliton propagation *Phys. Lett.* A **374** 3216
[39] Alam M S, Masud M M and Mamun A A 2013 Effects of bi-kappa distributed electrons on dust-ion-acoustic shock waves in dusty superthermal plasmas *Chin. Phys. B* **22** 115202
[40] Bostrom R 1992 Observations of weak double layers on auroral field lines *IEEE Trans. Plasma Sci.* **20** 756
[41] Lundin R, Eliasson L, Hultqvist B and Stasiewicz K 1987 Plasma energization on auroral field lines as observed by the Viking spacecraft *Geophys. Res. Lett.* **14** 443
[42] Hall D, Chaloner C P, Bryant D A, Lepine D R and Trikakis J 1991 Electrons in the boundary layers near the dayside magnetopause *J. Geophys. Res.* **96** 7869
[43] Asbridge J R, Bame S J and Strong I B 1968 Outward flow of protons from the earth's bow shock *J. Geophys. Res.* **73** 5777
[44] Mouhammadoul B B, Tiofack C G L, Alim A and Mohamadou A 2021 Positron-acoustic traveling waves solutions and quasi-periodic route to chaos in magnetoplasmas featuring Cairns nonthermal distribution *Eur. Phys. J. D* **75** 61
[45] Lundin R, Zakharov A, Pellinen R, Borg H, Hultqvist B, Pissarenko N, Dubinin E M, Barabash S W, Liede I and Koskinen H 1989 First measurements of the ionospheric plasma escape from Mars *Nature London* **341** 609
[46] Pillay S R and Verheest F 2005 Effect of non-thermal ion distributions on the Jeans instability in dusty plasmas *J. Plasma Phys.* **71** 177
[47] Annou K and Annou R 2012 Dromion in space and laboratory dusty plasma *Phys. Plasmas* **19** 043705
[48] Panguetna C S, Tabi C B and Kofané T C 2017 Two-dimensional modulated ion-acoustic excitations in electronegative plasmas *Phys. Plasmas* **24** 092114
[49] Tabi C B, Panguetna C S and Kofané T C 2018 Electronegative (3+1)-dimensional modulated excitations in plasmas *Physica B* **545** 370
[50] Bedi C and Gill T S 2012 Study of envelope electron acoustic solitary waves under transverse perturbations having kappa distributed hot electrons *Phys. Plasmas* **19** 062109
[51] Jianping S, Jibin L and Shumin L 2013 Analytical travelling wave solutions and parameter analysis for the (2+ 1)-dimensional Davey–Stewartson-type equations PRAMANA *J. Phys* **81** 747
[52] Cairns R A, Mamun A A, Bingham R, Bostrom R, Dendy R O, Nairn C M C and Shukla P K 1995 Electrostatic solitary structures in non-thermal plasmas *Geophys. Res. Lett.* **22** 2709
[53] Mamun A A, Cairns R A and Shukla P K 1996 Effects of vortex-like and non-thermal ion distributions on non-linear dust-acoustic waves *Phys. Plasmas* **3** 2610
[54] Rahman M M, Alam M S and Mamun A A 2014 Positron-acoustic Gardner solitons and double layers in electron-positron-ion plasmas with nonthermal electrons and positrons *Eur. Phys. J. Plus* **129** 84
[55] Paul I, Chandra S, Chattopadhyay S and Paul S N 2016 W-type ion-acoustic solitary waves in plasma consisting of cold ions and nonthermal electrons *Indian J. Phys.* **90** 1195
[56] Rahman M M, Mamun A A and Alam M S 2014 Positron acoustic shock waves in four-component plasmas with nonthermal electrons and positrons *J. Korean Phys. Soc.* **64** 1828
[57] Chowdhury N A, Mannan A, Hossen M R and Mamun A A 2018 Modulational instability and generation of envelope solitons in four-component space plasmas *Contrib. Plasma Phys.* **58** 870
[58] Taniuti T and Yajima N 1969 Perturbation method for a nonlinear wave modulation *I. J. Math. Phys.* **10** 1369
[59] Davey A and Stewartson K 1974 On three-dimensional packets of surface waves *Proc. R. Soc. London, Ser. A* **338** 101
[60] Wazwaz A M, Weaam A and Samir E-T 2024 Study of a combined Kairat-II-X equation: Painlevé integrability, multiple kink, lump and other physical solutions *Int. J. Numer. Methods Heat Fluid Flow* **34** 3715–30
[61] Wazwaz A M, Alhejaili W, Matoog R T and El-Tantawy S A 2024 Painlevé integrability and multiple soliton solutions for the extensions of the (modified) Korteweg–de Vries-type equations with second-order time-derivative *Alexandria Eng. J.* **103** 393–401
[62] Wazwaz A M, Alhejaili W and El-Tantawy S A 2024 Integrability and multiple kinks, lumps, and breathers solutions to an extended (3+1)-dimensional Calogero–Bogoyavlenskii–Schiff fluid model *Phys. Scr.* **99** 095228
[63] Wazwaz A M, Alhejaili W and El-Tantawy S A 2024 On the Painlevé integrability and nonlinear structures to a (3+1)-dimensional Boussinesq-type equation in fluid mediums: Lumps and multiple soliton/shock solutions *Phys. Fluids* **36** 033116
[64] Wazwaz A M, Alhejaili W and El-Tantawy S A 2023 Physical multiple shock solutions to the integrability of linear structures of Burgers hierarchy *Phys. Fluids* **35** 123101
[65] Wazwaz A M, Mansoor A and El-Tantawy S A 2023 Study on (3+1)-dimensional nonlocal Boussinesq equation: Multiple soliton solutions *Int. J. Numer. Methods Heat Fluid Flow* **33** 4090–100
[66] Wazwaz A M, Alhejaili W, Matoog R T and El-Tantawy S A 2023 On the Painlevé integrability of three-extensions to Mikhailov–Novikov–Wang equations: Multiple solitons, shocks, and other physical solutions *Phys. Fluids* **35** 113114
[67] Wazwaz A M, Alhejaili W and El-Tantawy S A 2023 Analytical study on two new (3+1)-dimensional Painlevé integrable equations: Kink, lump, and multiple soliton solutions in fluid mediums *Phys. Fluids* **35** 093119
[68] Wazwaz A M, Alhejaili W and El-Tantawy S A 2023 Study on extensions of (modified) Korteweg–de Vries equations: Painlevé integrability and multiple soliton solutions in fluid mediums *Phys. Fluids* **35** 093110
[69] Wazwaz A M, Hammad M, Abu, Al-Ghamdi A O, Alshehri M H and El-Tantawy S A 2023 New (3+1)-dimensional Kadomtsev–Petviashvili–Sawada–Kotera–Ramani equation: multiple-soliton and lump solutions *Mathematics* **11** 3395
[70] Wesson J T 2004 *Tokamaks* (Oxford University Press)